Evolutionary algorithm to design high-cooperativity optical cavities

D. V. Karpov, P. Horak

Optoelectronics Research Centre, University of Southampton, Southampton SO17 1BJ, United Kingdom

E-mail: d.karpov@soton.ac.uk

Abstract. Using an evolutionary algorithm combined with a gradient descent method we design optical cavities with significantly enhanced strong coupling rates between cavity photons and a single quantum emitter. Our approach allows us to find specially designed non-spherical mirrors which lead to high-finesse cavity eigenmodes with large field enhancement at the center of the cavity. The method is based on adding consecutive perturbations to an initial spherical mirror shape using the gradient descent method for optimization. We present mirror profiles which demonstrate higher cavity cooperativity than any spherical cavity of the same size. Finally, we demonstrate numerically how such a cavity enhances the operation frequency and purity of coupling a Ca^+ ion to an optical fiber photon.

1. Introduction

Strong coupling of a quantum emitter, e.g., an ion, atom, NV-center, or quantum dot, to an optical mode of a resonator and long cavity photon lifetime are essential in numerous applications of quantum optics for fundamental research and for practical quantum technology. Promising systems to fulfill these requirements are fiber-optic microcavities [1–4], ion beam etched dielectric resonators [5], or micro-assembled structures [6].

Strong coupling between emitter and cavity photon can be realized by a small cavity volume and therefore by a very short optical cavity. However, for many realistic quantum setups the cavity mirrors cannot be placed too close to each other due to technical difficulties: for trapped ion systems, short cavities lead to electrical charging of the dielectric mirrors and to distortion of the radio frequency ion trapping fields [7]; for neutral atoms, short cavity lengths are limited by the requirement for delivery of atoms into the cavity and for optical side access [8, 9] for cooling and trapping. Thus, optical cavities utilized in quantum optical device applications need to combine a strong coupling rate with low losses while keeping the mirrors sufficiently apart.

One way to achieve strong coupling is to operate the cavity in a (near-) concentric configuration [10]. This minimizes the optical mode field waist at the cavity center, thus maximizing emitter-photon coupling, but at the cost of increased clipping losses because of a large mode field diameter on the mirrors which limits the maximum achievable cavity performance as given by the cavity cooperativity.

Another method to increase the field amplitude in the center of the cavity is the creation of some interference pattern by modulating the mirror profile [11]. We assume that we are not limited by spherical cavities, i.e., we can create an arbitrary mirror shape using, for example, focused ion beam milling or laser ablation as discussed in more detail in Sec. 6. Here, we numerically explore modulated spherical profiles of the cavity mirrors which give rise to highly localized cavity modes while at the same time keeping losses low. With this approach we find a manifold of mirror profiles which can provide a lower loss rate than a concentric cavity, thus achieving higher cooperativity. In contrast to our earlier work [11], here we do not require a priori knowledge of the exact mode shape we want to generate (in particular, specific superpositions of many Laguerre-Gaussian modes), but the numerical algorithm directly uses the mirror shape for optimization without restrictions on the mode fields. As we will see, this approach can achieve comparable cooperativity for much simpler mirror shapes.

The goal of our work here is to present a procedure based on an evolutionary algorithm which allows us to design mirror shapes for optical cavities with higher coupling and cooperativity compared to spherical cavity mirrors of the same size. We then apply the method to optimize a fiber-tip cavity by also taking into account out-coupling of a cavity photon into an optical fiber, This yields a (slightly) larger overall transfer efficiency of an ion excitation to a fiber photon, but significantly increases the operating repetition frequency of such a device.

Evolutionary or genetic algorithms are used for various applications mostly for

inverse design problems [12, 13] and have also been applied in the field of modern optics [14–16]. In forward design of optical cavities, for given geometry and boundary conditions the corresponding cavity optical field can be calculated by highly developed and well known numerical, semi-analytical or analytical methods. However, it is not often possible to find parameters to create a target optical field distribution using forward design methods. Here we demonstrate a method which is based on consecutive "mutations" of an initial spherical mirror shape while calculating the mode spectrum and conducting gradient descent to optimize the mutations. The method allows us to find mirror profiles which provide significant enhancement of a target parameter, such as the cavity cooperativity.

This paper is organized as follows. First, in Sec. 2 we describe the problem under investigation, our motivation, theoretical model and optimization parameters. In Sec. 3 we describe the algorithm and the role of the gradient descent method in it. In Sec. 4 we present the results of our simulations, in particular the cavity mode topology, strong coupling rate, and cooperativity enhancement factor, and we investigate the alignment sensitivity of our cavity designs. In Sec. 5 we apply our method for coupling a Ca^+ ion in a Λ-scheme via a fiber-tip cavity to an optical fiber photon and demonstrate the significantly faster time evolution of the improved system. Finally, we briefly discuss fabrication opportunities to realize such mirrors experimentally and conclude in Sec. 6.

2. Problem statement

The coherent coupling between a quantum emitter, such as a quantum dot, ion or cold atom, located at a coordinate $\mathbf{r}$ in an cavity with a dimensionless optical field mode $\psi(\mathbf{r})$ is characterized by the strong coupling rate [17]

$$g_0(\mathbf{r}) = \sqrt{\frac{3\lambda^2 c\Gamma}{4\pi V_\psi}}\psi(\mathbf{r}) = g_0(\mathbf{r}_m)\psi(\mathbf{r}), \quad \psi(\mathbf{r}) = \frac{E(\mathbf{r})}{|E(\mathbf{r}_m)|} \tag{1}$$

where $E(\mathbf{r})$, Γ, λ, $\mathbf{r}_m$ are electric field of the cavity mode, the spontaneous decay rate of the emitter $\Gamma = \frac{\omega^3\mu^2}{3\pi\varepsilon_0\hbar c^3}$ (where ω is the transition angular frequency and μ is the electric dipole moment), its transition wavelength, and the maximum electric field intensity point, respectively. Here we assume that the emitter dipole moment and the electric field polarization vectors are aligned. The cavity mode volume V_ψ is given by

$$V_\psi = \int_{V_{cavity}} |\psi(\mathbf{r})|^2 dV. \tag{2}$$

If the emitter-cavity strong coupling rate g_0 is larger than the strength of any incoherent processes, i.e., than the decay rate Γ and the loss rate κ of the cavity field, the cavity operates in the strong coupling regime. In this case the cooperativity parameter C_0 at the field maximum,

$$C_0 = \frac{g_0^2(\mathbf{r}_m)}{\kappa\Gamma} = \frac{3\lambda^2 c}{4\pi\kappa V_\psi}, \tag{3}$$

is larger than one.

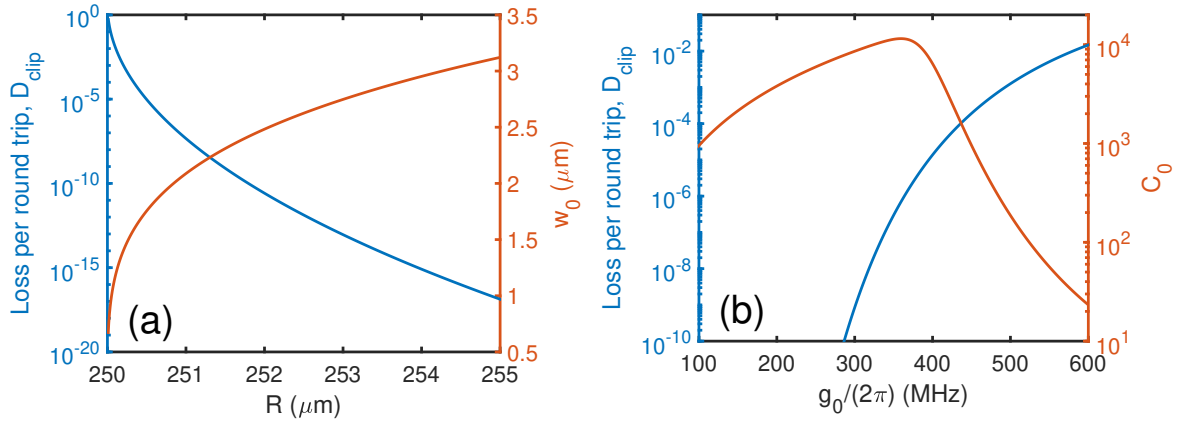

Figure 1: (a) Clipping losses D_{clip} and focal waist w_0 versus mirror radius of curvature for a spherical cavity near the concentric limit. Cavity parameters are $L = 500$ μm and mirror diameter 200 μm. (b) D_{clip} and cooperativity C_0 corresponding to (a) plotted versus the coupling rate g_0 for a Ca^+ ion with $\Gamma_{Ca^+} = 2\pi \times 22$ MHz, $D_{abs} = 10^{-5}$.

We consider two contributions to the cavity loss rate κ. The first is transmission of light through the cavity mirrors or absorption within them with a corresponding loss per round trip of typically $D_{abs} = 10^{-5} \leftrightarrow 10^{-3}$. The second contribution is clipping losses D_{clip} coming from light of the cavity mode which misses the cavity mirrors due to their finite diameter. The cavity decay rate κ and the corresponding cavity finesse F are given by

$$\kappa = \frac{c}{2L}(D_{clip} + D_{abs}) = \frac{c\pi}{L}\frac{1}{F}. \tag{4}$$

2.1. Concentric cavity limit

As mentioned above, one way to enhance the cavity field at the center is to operate a spherical mirror cavity near the concentric limit. In this case, the mode volume of the fundamental Laguerre-Gaussian mode is $V_\psi = \frac{\pi}{4} w_0^2 L$, where w_0 is the waist at the focus and L the cavity length, and the cooperativity C_0, Eq. (3), can be rewritten as [10]

$$C_0 = \frac{3\lambda^2 c}{\pi^2 \kappa w_0^2 L} = \frac{6\lambda F}{\sqrt{2RL - L^2}} \tag{5}$$

where R is the radius of curvature of the mirrors. C_0 thus increases significantly for $R \to L/2$, the concentric limit. (Note that Eq. (5) is valid in the paraxial approximation and breaks down when the waist approaches the wavelength.) The strong coupling rate scales as $g_0 \sim 1/w_0$. However, as the waist is reduced, the spot size on the mirror (in the far field, $L/2 \gg$ Rayleigh length) scales with $1/w_0$ and thus linearly with g_0. Hence, the clipping losses increase dramatically for stronger coupling.

Figure 1 shows a numerical example of the scaling of the cavity parameters in the concentric limit. Figure 1(a) plots the loss per round trip (blue curve) and Gaussian beam waist (red curve) as a function of radius of curvature for the fundamental cavity

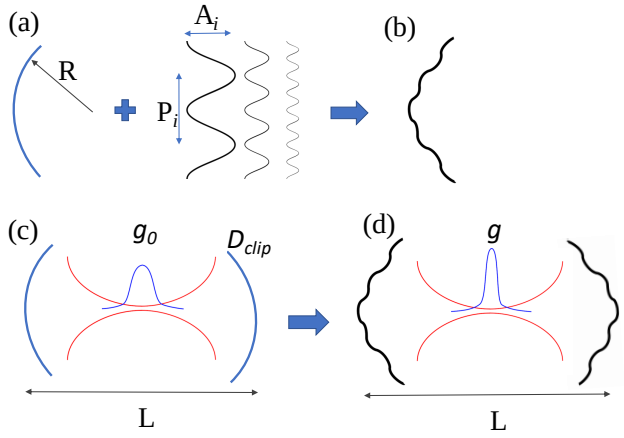

Figure 2: Schematic of our cavity optimization scheme. (a) and (b) show the mirror modification process by adding harmonic modulations to a spherical shape. (c) and (d) indicate the cavity mode divergence by the red curves and the local field enhancement resulting from the created interference pattern by the blue Gaussian-like curves.

mode. As $R \to L/2 = 250\,\mu$m, the waist decreases in the center but simultaneously the mode on the mirror increases and thus clipping losses increase due to the finite mirror diameter. In Fig. 1 (b) we re-plot the clipping loss versus the coupling rate g_0 (proportional to $1/w_0$ from figure (a)) which shows the increasing loss with increasing g_0. The black curve shows the corresponding cooperativity C_0: it first increases as g_0 increases but then rapidly falls when the spot size on the mirror exceeds the mirror diameter, thus exhibiting a clear maximum of cooperativity that can be achieved with spherical mirror cavities.

2.2. Strong coupling rate and cooperativity enhancement by optimized cavity designs

The goal of this paper is to overcome the limits found in Fig. 1 for the cooperativity by allowing for non-spherical mirrors and using an evolutionary algorithm to optimize the shape of the mirrors. We thereby aim to increase the coupling rate g_0 by local field enhancement, but without the excessive clipping losses found in the concentric limit.

A schematic of this approach is shown in Fig. 2. We start by choosing an appropriate spherical mirror cavity with given mirror radius of curvature and cavity length, which we use as a reference cavity. We then alter the mirror profiles, as depicted in Fig. 2, and calculate the corresponding mode field Ψ which we normalize to the maximum of the reference field ψ. Thus, Ψ is the field enhancement relative to the reference cavity and we have the corresponding strong coupling rate

$$g(\mathbf{r}) = \sqrt{\frac{3\lambda^2 c\Gamma}{4\pi V_\psi}}\Psi(\mathbf{r}) = g_0(\mathbf{r}_m)\Psi(\mathbf{r}) \tag{6}$$

Likewise, the cooperativity C in the center becomes

$$C = \frac{g^2}{\kappa_\Psi \Gamma} = \frac{3\lambda^2 c}{4\pi} \frac{\Psi(\mathbf{r}_m)^2}{\kappa_\Psi V_\psi} = C_0 \frac{\kappa}{\kappa_\Psi} \Psi(\mathbf{r}_m)^2 \tag{7}$$

where κ_Ψ is the cavity loss rate of the modified mode Ψ. Therefore, the cooperativity is increased by the field enhancement and/or if the cavity loss is reduced. Finally, if we assume that the reference cavity has negligible clipping losses and that mirror transmission and absorption D_{abs} is the same for the reference and modified cavities, we can express the enhancement of cooperativity as

$$\frac{C}{C_0} = \frac{1}{\frac{D_{clip}}{D_{abs}} + 1} \Psi(\mathbf{r}_m)^2 \tag{8}$$

where D_{clip} here refers to the clipping loss of the modified cavity.

3. Evolutionary algorithm

We consider a cylindrically symmetric cavity where the mirror profile $Z(r)$ consists of a sphere with radius of curvature R and some harmonic perturbations with amplitude A_i and period P_i. We work in the paraxial limit and thus can replace the spherical profile by a parabola, leading to a modified profile described by

$$Z(r) = \frac{r^2}{2R} + \sum_i A_i \cos(r/P_i). \tag{9}$$

The purpose of this is to create some interference pattern and to enhance the mode field in the center $\Psi(\mathbf{r}_m)$ but at the same time we want to avoid creating large clipping losses on the mirror D_{clip}. Figure 2 gives a schematic of the scheme.

For the numerical evaluation and optimization of our scheme we require a *Solver* function that takes the mirror geometry as an argument and returns the cavity modes and their clipping losses, from which we select the mode with the highest cooperativity,

$$Z(r) \Rightarrow Solver(Z) \Rightarrow \Psi(\mathbf{r}_m, z), D_{clip} \Rightarrow C. \tag{10}$$

The *Solver* could be any numerical or analytic method. In this paper we implemented the solver using a mode mixing method (MMM) [11,18,19] in the paraxial approximation [20].

A schematic of our algorithm is presented in Fig. 3. We start with one mutation, i.e., one harmonic modulation of the mirror, represented by a couple of parameters $\theta = (A, P)$. Several instances of this geometry are then created and every instance is modified by adding a small, individual perturbation $\epsilon = (\delta A, \delta P)$ which is drawn randomly from a 2-dimensional normal distribution $N(0, \sigma_A, \sigma_P)$ with zero mean and standard deviations σ_A, σ_P. For every instance, the *Solver* is then applied to find the cooperativity C for the geometry $(\theta + \epsilon)$. The results are then combined for a gradient descent method (GD) where we compute the derivative by a probability approach used in variations analysis [21, 22],

$$\nabla C(\theta) \approx \frac{1}{\sigma_A^2 \sigma_P^2} \mathbb{E}_{\epsilon \sim N(0,\sigma_A,\sigma_P)}[\epsilon C(\theta + \epsilon)], \tag{11}$$

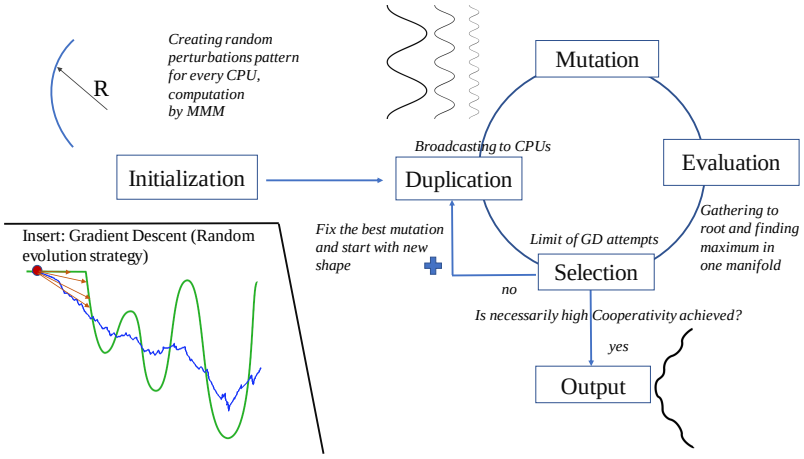

Figure 3: Schematic of the evolutionary algorithm and the gradient descent method with random evolution implementation.

where $\mathbb{E}$ is the expectation value over the normal distribution. Once the GD is converged we fix this mutation, i.e., we fix the harmonic modulation (A_1, P_1), and add a second perturbation (A_2, P_2) which is then again optimized by GD as before. This continues until satisfactory performance of the cavity is found.

The random evolution GD is graphically shown in the insert of Fig. 3. The algorithm introduces some stochasticity to the results but adds significant advantages, such as the possibility to move through flat areas (when the classical gradient is zero) and to go through walls and local minima. Note that this approach includes the main features of more standard genetic algorithms: "mutation" is present through the generation of many instances distributed around the mean value with a normal distribution; "reproduction" is performed by the gradient descent step based on the average of the entire pool of instances, thus the periodic modulations of the next generation of instances depend on modulations of all instances in the parent generation; this step therefore also includes a type of "blend crossover" but it is not based on two individual instances of the parent generation but on the full population. The algorithm is also easily implemented for parallel computing with an effectiveness that grows almost linearly with computational resources [21, 22]. Our home-mode computer program was written in Python using the libraries numpy for computation and mpi4py for distribution over a multicore processor.

4. Results and discussion

We present an example of our results in Fig. 4. Here a mirror surface with 5 harmonic mutations has been found by optimization with the evolutionary algorithm described in Sec. 3. The spherical reference cavity has a length of $L = 500$ μm, mirror radius of curvature $R = 400$ μm, and the operating wavelength is set to $\lambda = 0.866$ μm. The algorithm made mutations of the spherical shape with harmonic amplitudes and periods in the ranges $A_i = 0.1 - 0.5$ μm and $P_i = 10 - 30$ μm, respectively.

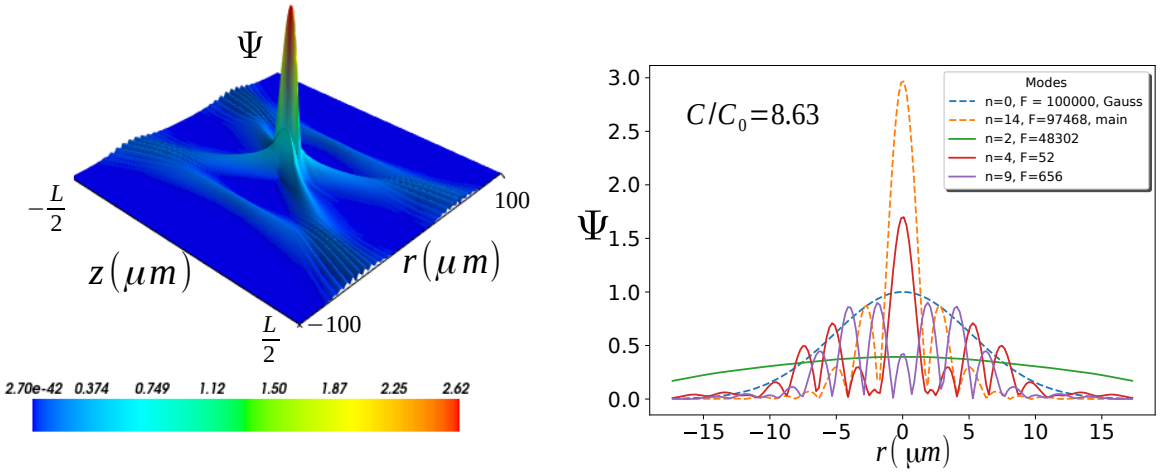

(a) (b)

Figure 4: (a) High cooperativity mode field $\Psi(r, z)$ for mirrors optimized by the evolutionary algorithm. (b) Cross sections of several eigenmodes of the same cavity, with corresponding cavity finesse F given in the legend. The dashed curve corresponds to the fundamental mode of spherical reference cavity with parameters $L = 500$ μm, $R = 400$ μm.

The optimized eigenmode Ψ with the highest cooperativity mode is shown in Fig. 4(a) and the cross section in the center by the orange curve in Fig. 4(b). For comparison, the fundamental Laguerre-Gaussian mode of the spherical reference cavity is depicted by the blue dashed line. The figure clearly shows the field enhancement achieved in the center. At the same time, for the optimized mode the clipping loss has not increased significantly and thus the cooperativity, Eq. (8), has been increased by a factor of 8.63. The cavity with the optimized mirror shapes also supports other eigenmodes, some of which are shown in Fig. 4(b); these modes have larger clipping losses and thus lower finesse, see the legend of the figure. Note that there is no unique way of defining the order of eigenmodes in such a complex mirror geometry and thus the eigenmode index n is arbitrarily determined by the *Solver*.

We can clearly see that the designed superposition of harmonic perturbations on the spherical mirror shapes provides a cavity eigenmode with significant strong coupling enhancement but moderate low losses. This is a valuable enhancement for quantum optics and quantum engineering applications; a specific example will be discussed in more detail in Sec. 5.

We want to comment briefly on the convergence properties of our chosen algorithm. In standard GD methods depending on the choice of initial parameters the algorithm often converges to a local minimum instead of an overall, global optimum. Here we eliminate this issue by two approaches. First, we produce a superposition of mutations. Thus, if in one mutation the algorithm gets stuck in a local minimum, this is mitigated by another starting point in the next mutation. Second, we compute the gradient using

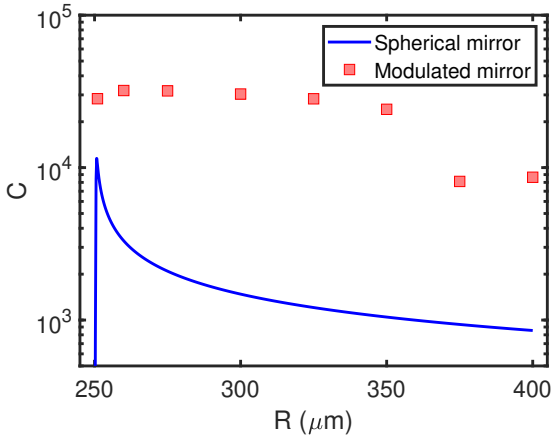

Figure 5: Comparison of cooperativities C achieved by our evolutionary algorithm (red squares) with those of spherical cavities (blue curve). Parameters as in Fig. 1.

the probabilistic derivative of Eq. (11), which allows the algorithm to move through flat areas and through walls, see insert in Fig. 3 and references [21, 22].

In Fig. 4 we demonstrated an enhancement factor of 8.63 for the cooperativity relative to a spherical reference cavity deep in the stable cavity regime, i.e., far away from the concentric limit $R = L/2$. This optimization was easily achieved on an 8-core processor, where the algorithm made 5 mutations and fewer than 20 iterations in every GD procedure. However, the efficiency of the algorithm and the achievable cooperativity enhancement depend on how close the reference cavity is to the concentric geometry. In Fig. 5 we therefore show more numerical results of cooperativity enhancement achieved with our method by modulated spherical mirrors (red squares) compared to spherical cavities approaching the concentric limit (blue curve). We see that our approach provides significantly higher cooperativity over a very wide range of parameters. In fact, we notice that the cooperativities achieved with modulated mirrors are higher than can be achieved with spherical mirrors for any radius of curvature. Thus we can significantly exceed the limit for spherical cavities of $C \simeq 1.15 \times 10^4$ for the parameters of Fig. 5 set by the large clipping losses close to the concentric regime, as discussed in Fig. 1.

Near-concentric cavities are known to be sensitive to alignment errors, so it is interesting to investigate how accurately the modulated-mirror cavities must be aligned. We therefore performed a series of numerical simulations to calculate the modes of cavities that are misaligned by a lateral shift Δx or by a tilt angle $\Delta\alpha$ between the two mirrors, with the results shown in Fig. 6.

We expect this alignment sensitivity to depend on the complexity of the mirror deformation and on the achieved cooperativity enhancement. We therefore select three mirror shapes, with superpositions of one, two, and three periodic modulations, respectively. Each mirror shape was obtained by numerical optimization as discussed above. The deviations of the optimized mirror shapes from spherical, i.e. the summation

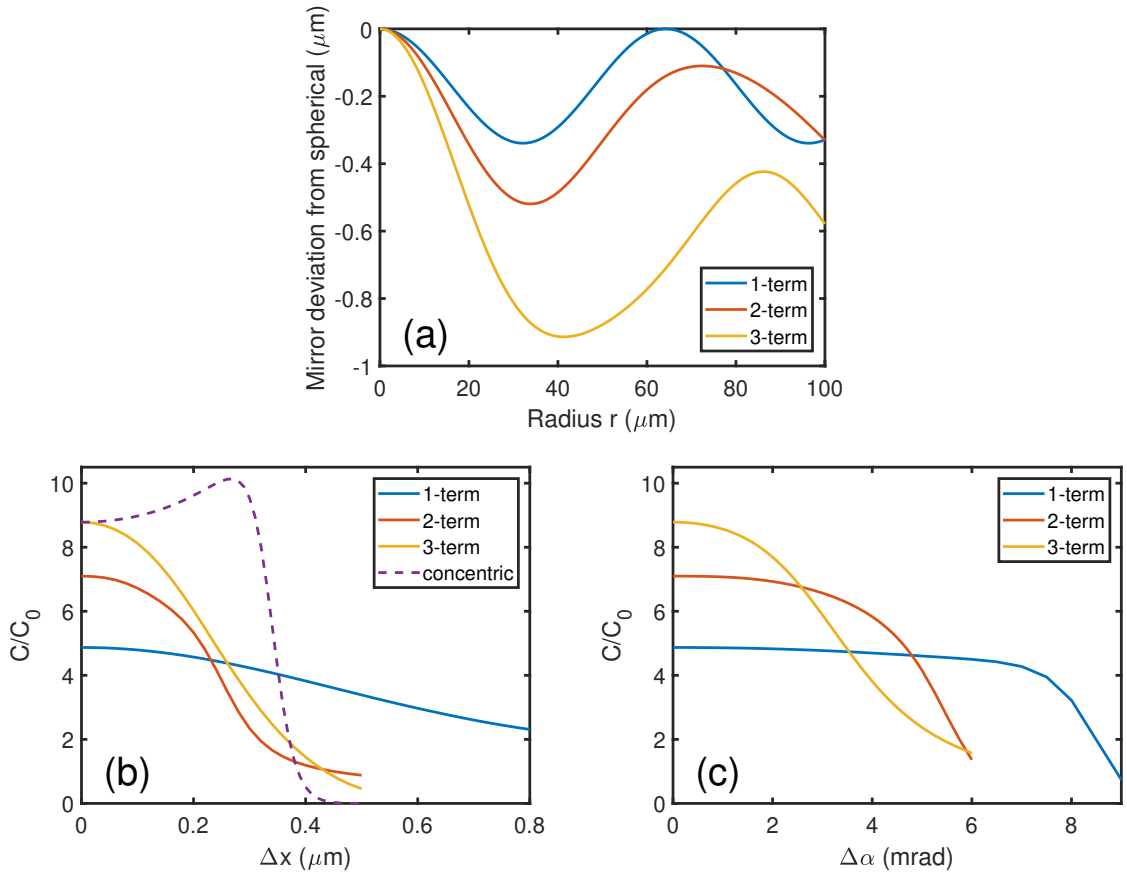

Figure 6: Alignment sensitivity of our cavity designs. (a) Deviation from spherical profile for three optimized mirror designs with 1, 2, 3 periodic terms, respectively. (b) Corresponding cooperativity C versus transverse misalignment of cavity, and (c) cooperativity versus angular misalignment of cavity with $D_{abs} = 10^{-5}$, $L = 500$ μm, $R = 400$ μm. In (b) we also show C versus misalignment for a near-concentric spherical cavity ($R = 251.944\,\mu$m).

terms in Eq. (9), are shown in Fig. 6(a). For perfect cavity alignment the three mirrors yield a cooperativity enhancement of $C/C_0 = 4.87$, 7.10, 8.78, respectively. Note that using the results of Ref. [11] much more complicated mirror shapes requiring the superposition of 5, 7, and 9 Laguerre polynomials would be required to achieve the same cooperativity enhancement.

The dependence of C/C_0 versus linear lateral displacement of the mirrors is shown in Fig. 6(b). As expected, C/C_0 decreases as Δx increases and reaches half the original cooperativity at displacements of 0.75, 0.26, and 0.26 μm. The alignment sensitivity of a near-concentric spherical cavity with the same cooperativity of C/C_0 as the 3-term mirror shape is 0.36 μm (dashed curve). Here C first increases as the cavity length slightly increases with misalignment before dropping of quickly. The sensitivity of our cavity designs to a tilt angle between the mirrors is shown in Fig. 6(c). Here the point of half cooperativity is reached at angles of $\Delta\alpha = 8.30$, 5.22, and 3.70 mrad, respectively.

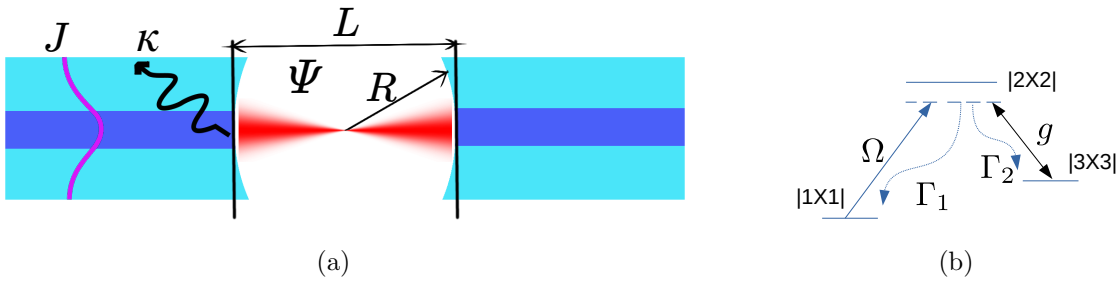

(a) (b)

Figure 7: (a) Coupling of a mode from a fiber tip optical cavity to an optical fiber mode. J (pink curve) represents the fiber mode, Ψ (red) the cavity mode, κ the cavity loss rate, L and R the cavity length and mirror radius of curvature, respectively. (b) Λ-level scheme of the ion under investigation.

A corresponding near-concentric cavity is much more stable with respect to mirror tilt with a half width of $\Delta\alpha = 272$ mrad as long as the two mirror centers of curvature remain exactly on the cavity axis.

In our numerical experiments we have observed a significant dependence of the misalignment tolerances on the actual mirror shapes. For example, we have also found mirror shapes that are *less* sensitive to alignment than near-concentric cavities of the same cooperativity. We conclude that, while in general the alignment sensitivity is of the same order of magnitude as for concentric cavities, in future realistic cavity optimizations using our method this should be taken into account in the optimization routine.

5. Application to quantum state transfer

5.1. Coupling to a fiber mode

The same evolutionary algorithm used above for the enhancement of cavity cooperativity can be applied for the optimization of any parameter. As an example relevant for quantum information processing, we will investigate the state transfer of an ion in Λ-configuration to a single photon in an optical fiber.

The ion is trapped inside a fiber-tip cavity [23–25]. High cooperativity is required to transfer the ion state to a cavity photon, but good mode matching between the cavity mode through the mirror into the optical fiber mode is also necessary to optimize the outcoupling from the cavity, see Fig. 7(a). Thus, the spot size as well as the curvature of the wave front of the cavity mode at the mirror should match those of the optical fiber. To determine the mode overlap we calculate the mode matching integral η between the fundamental mode $\Psi(r)$ of the cavity and the output field $J(r)$ of a single-mode fiber,

$$\eta = \frac{|\int \Psi(r) J^*(r)\, r dr|^2}{\int |\Psi(r)|^2\, r dr \int |J(r)|^2\, r dr} \tag{12}$$

where the integration over the mirror surface is changed to an integration along the line at $z = L/2$ from 0 to the edge of the fiber in the paraxial approximation. Note

that for spherical cavities η can approach 1 with the help of mode matching optics [24], but to maximize coupling from the ion to the cavity and from the cavity to the fiber simultaneously we are interested in optimizing a combination of cooperativty C and overlap η, which can be done by the same evolutionary algorithm presented in Sec. 3. Below we demonstrate this explicitly for a Λ-scheme with a calcium ion in a fiber cavity.

5.2. Λ-scheme

We consider a three level Ca^+ ion [26] in a Λ-configuration as shown in Fig. 7(b). This configuration is promising for high-fidelity quantum computing and quantum communication [27–30]. The system consists of two ground levels $|1\rangle, |3\rangle$ and an excited level $|2\rangle$. Raman transitions are induced by a coherent pump on the transition $|1\rangle - |2\rangle$ and the cavity mode which couples to the transition $|3\rangle - |2\rangle$. The Hamiltonian describing the coherent system dynamics is given by

$$H = \Delta |2\rangle \langle 2| - \Delta |3\rangle \langle 3| + ig(a^+\sigma_3 - a\sigma_3^+) + i\Omega(\sigma_1 - \sigma_1^+) \tag{13}$$

where $\sigma_3 = |2\rangle \langle 3|, \sigma_1 = |2\rangle \langle 1|$ are the transitions operators, a is the cavity photon operator, Δ, g and Ω are detuning, strong coupling rate and coherent pumping, respectively. Incoherent decays are given by the dissipation operators

$$\nu = \{\sqrt{\Gamma_1}\sigma_1, \sqrt{\Gamma_2}\sigma_3, \sqrt{\kappa}a\} \tag{14}$$

where Γ_1, Γ_2 and κ are spontaneous decay rates of $|2\rangle$ to $|1\rangle$, $|3\rangle$ and cavity linewidth, respectively. We thus solve the master equation for the density matrix ρ,

$$\frac{d\rho}{dt} = -\frac{i}{\hbar}[H, \rho] + \sum_\nu L(\rho, \nu) \tag{15}$$

where L is the Lindblad superoperator given by

$$L(\rho, \nu) = \nu\rho\nu^+ - \frac{1}{2}(\rho\nu^+\nu + \nu^+\nu\rho). \tag{16}$$

For this Λ-system the expression for the cavity cooperativity needs to be corrected to

$$C = \frac{\Gamma_2}{\Gamma_1}\frac{3\lambda^2 c}{4\pi}\frac{\Psi(\mathbf{r}_m)^2}{\kappa V_\Psi} \tag{17}$$

since we cannot eliminate Γ in Eq. (7) because of the two different decay channels of the excited state $|2\rangle$. The branching ratio for Ca^+ is $\Gamma_2/\Gamma_1 \approx 0.1$, thus reducing the cooperativity by a factor 10,

$$\frac{C}{C_0} = \frac{1}{\frac{D_{clip}}{D_{abs}} + 1}\frac{\Gamma_2}{\Gamma_1}\Psi(\mathbf{r}_m)^2. \tag{18}$$

The efficiency of converting the ion ground state into a fiber photon is given by a combination of photon emission probability into the cavity mode P_e and mode coupling efficiency η, Eq. (12). High efficiency is possible in the bad cavity regime, $\kappa \gg g^2/\kappa \gg \Gamma$, if the losses D_{abs} provide coupling of the cavity mode into the fiber mode and are larger than the undesired clipping losses D_{clip}. In this case and for sufficiently large time, the

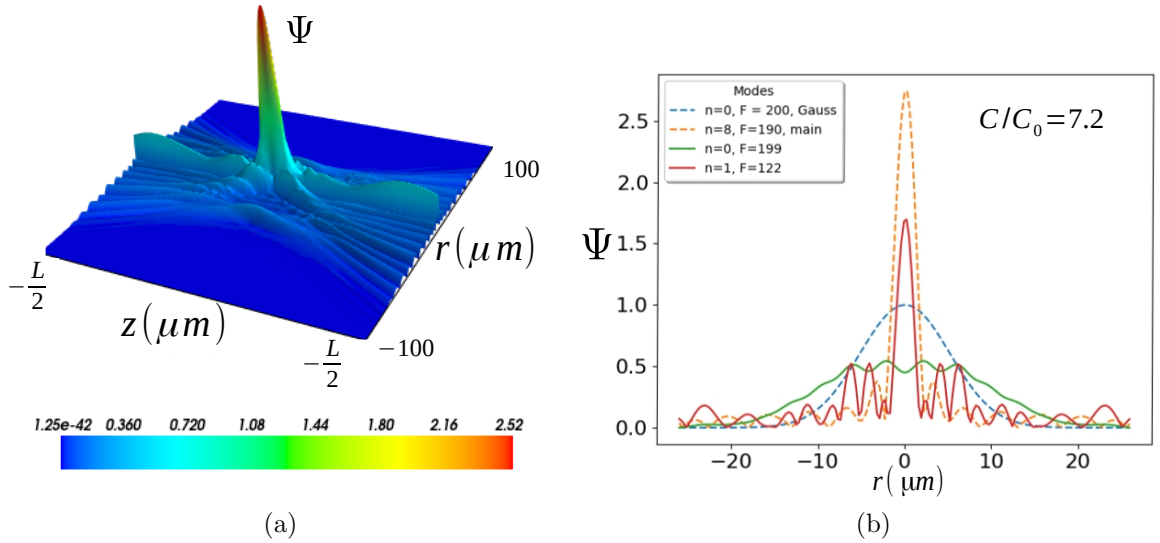

(a) (b)

Figure 8: (a) Optimized cavity mode field $\Psi(r, z)$ and (b) various cavity mode cross sections, similar to Fig. 4 but optimized for maximum overall ion to fiber state transfer probability O. Parameters as in Fig. 4.

photon emission probability is $P_e = \frac{C}{1+C}$ and the total efficiency O of generating a fiber photon becomes [31]:

$$O = P_e\eta = \frac{C}{1+C}\eta. \tag{19}$$

We can therefore use the evolutionary algorithm of Sec. 3 to design cavity modes for an optimized total efficiency O. We will then use the full quantum model, Eqs. (13)-(16), to check and confirm our results.

As discussed above, this approach is most valuable when we are restricted by geometry and are not able to move mirrors close to each other for a more concentric configuration. We start our optimization again with a spherical reference cavity with the following parameters: $L = 500$ μm, $R = 400$ μm, $D_{abs} = 5 \cdot 10^{-3}$, $\Gamma_1 = 22 \cdot 10^6$ s^{-1}, $\Gamma_2/\Gamma_1 \approx 0.1$. This represents a fairly typical fibre-tip cavity coupled to a Ca^+ ion in the bad cavity limit. Assuming optimum fiber mode matching, $\eta_0 \approx 1$, the cooperativity of this system is $C_0 \approx 0.17$ and thus the ion-to-fiber coupling efficiency, Eq. (19), is $O_0 = 0.145$.

Using our evolutionary algorithm we can find a modification of the mirror shape to achieve cooperativity and total efficiency enhancement, see Fig. 8. Compared to the optimization of cooperativity alone, Fig. 4, we see that we still get field enhancement at the center of the cavity, but now the field also maintains a maximum at $r = 0$ on the mirrors for coupling into the fiber. The cooperativity has increased by $C/C_0 \approx 7.2$ compared to the reference cavity. The mode matching between cavity and fiber has reduced to $\eta \approx 0.386$ because the cavity field is no longer Gaussian, but the overall coupling efficiency has still increased to $O \approx 0.169$ from $O_0 \approx 0.145$. Note that the coupling efficiency of $\eta \approx 0.386$ is a vast enhancement compared to $\eta \approx 0.01$ for the

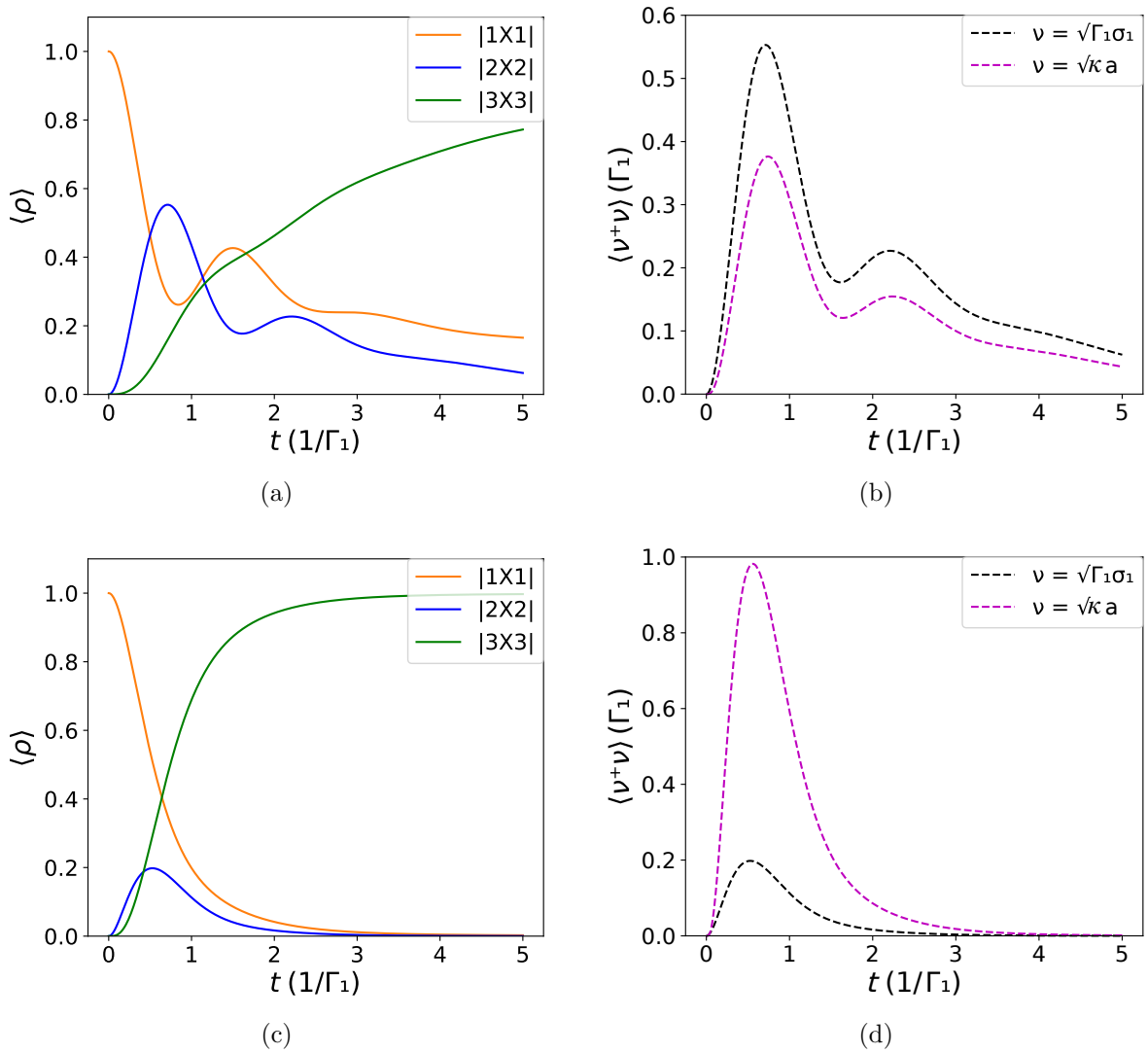

Figure 9: Quantum dynamics of the transfer of the ion ground state to a fiber photon. (a) and (c) are the ion energy level populations for the spherical reference cavity and for the optimized cavity, respectively. (b) and (d) show photon emission and spontaneous emission probabilities corresponding to (a) and (c), respectively. Parameters are $L = 500$ μm, $R = 400$ μm, $\kappa/\Gamma_1 = 68.18$, $\Delta/\Gamma_1 = 1$, $g/\Gamma_1 = 3.39$ for (a,b) and 10.17 for (c,d). The pump field is $\Omega/\Gamma_1 = 2$.

cavity of Fig. 4 optimized for cooperativity alone.

The dynamics of the quantum state transfer from the ion to a fiber photon for the reference cavity is shown in Fig. 9(a) and (b). The detuning Δ and laser Rabi frequency Ω are chosen to provide maximum efficiency for the fundamental Laguerre-Gaussian cavity eigenmode. The ion level populations are shown in Fig. 9(a): from the starting level $|1\rangle$ (orange line) we coherently excite the $|1\rangle \rightarrow |2\rangle$ transition, then via emission of a cavity photon the excited state $|2\rangle$ (blue line) is coupled to the second ground state $|3\rangle$

(green line). Fig. 9 (b) demonstrates the corresponding ion spontaneous emission (black dashed line) and cavity decay (pink dashed line). We observe that the unwanted ion decay probability is higher than the desired cavity decay because of a large population in the excited state $|2\rangle$, Fig. 9(a), and that the overall time scale of the state transfer is rather slow because of the relatively weak ion-cavity coupling g, thus resulting in a low operation frequency of the scheme.

Figures 9(c) and (d) show the equivalent quantum dynamics for the cavity mode that has been optimized with the evolutionary algorithm, Fig. 8. We note that while the total efficiency only slightly increased from 0.145 to $O \approx 0.169$, the quantum dynamics has changed dramatically compared to Figs. 9(c) and (d): the population of the excited state $|2\rangle$ is significantly suppressed by the faster coupling coefficient g, thus reducing the amount of unwanted spontaneous ion decay; the final population of $|3\rangle$ becomes almost 1 within the chosen time scale; and the whole dynamics occurs much faster, thus enabling a much faster processing time if such a scheme is employed in a quantum information processor.

Overall, we may therefore conclude that while our optimization of O has led to a reduction of the cavity to fiber mode coupling, we still gain a slight increase in the overall transfer efficiency, but even more importantly the achieved enhancement of ion-cavity coupling g allows for a several times faster operation speed.

6. Final comments and conclusions

We briefly comment here on possible experimental realizations of the mirrors designed in this paper. As we discussed in Sec. 3, the target mirrors are based on a spherical shape with added periodic modulations as a function of the radial coordinate r. We assume that these deviations are small enough to not create additional scattering losses but big enough to make fabrication possible. The typical range of perturbations predicted by our method are amplitudes of $A_i = 0.1 - 1$ μm and periods of $P_i = 1 - 100$ μm.

Such mirror machining can be achieved by many modern fabrication techniques. For example, we may shape the mirrors by laser ablation [32–34] or focused ion beam milling [5]. Pulses of a CO_2 laser can be used for thermal evaporation of surface material [23, 24] and laser radiation focused on the cleaved fiber ends can also produce surface qualities with extremely low roughness. Alternatively, modern micro-machining [35–37] can provide hundreds of nm precision which is sufficient for our range of parameters. Sinusoidal patterns might also be achieved by laser ablation techniques using interference of laser beams to generate the required patterns.

In conclusion, we have developed an approach based on evolutionary algorithm and gradient descent methods that allows us to design optimized optical cavities for quantum optics and quantum technology applications. We demonstrated designs that achieve significant enhancement of the strong coupling rate and the cooperativity beyond the limitations of spherical, near-concentric cavities. We further demonstrated the flexibility of our numerical approach by designing a fiber-tip cavity for optimized quantum state

transfer with a Λ-scheme in Ca^+ ions from the ion ground state to an optical fiber photon. This optimization not only led to enhancement of the transfer success rate, but also increased the operation speed of the scheme several times. We envisage that our evolutionary algorithm is applicable in many optimization problems that exhibit a large number of local minima.

Acknowledgments

We acknowledge financial support by the UK Quantum Technology Programme under the EPSRC Hub in Quantum Computing and Simulation (EP/T001062/1). The calculations were performed using the Iridis 5 supercomputer facilities at the University of Southampton.

Data availability statement

The data that support the findings of this study will be openly available at the following DOI: https://doi.org/10.5258/SOTON/D2246. The computer code of the evolutionary algorithm is available on request from the corresponding author (D.K.).

[1] Pellizzari T, Gardiner S, Cirac J and Zoller P 1995 *Phys. Rev. Lett.* **75** 3788–3791
[2] Cirac J I, Zoller P, Kimble H J and Mabuchi H 1997 *Phys. Rev. Lett.* **78** 3221–3224
[3] Kimble H J 2008 *Nature* **453** 1023–1030
[4] Monroe C and Kim J 2013 *Science* **339** 1164–1169
[5] Romagnoli P, Maeda M, Ward J M et al. 2020 *Appl. Phys. B* **126**, 111
[6] Bitarafan M H, DeCorby R G 2017 *Sensors (Basel)* **17** 1748
[7] Lucas D M et al. 2003 *Philos. Transact. A Math Phys Eng Sci.* **361**, 1401-8
[8] Harlander M, Brownnutt M, Hänsel W, R and Blatt R 2010 *New J. Phys.* **12** 093035
[9] Podoliak N, Takahashi H, Keller M and Horak P 2016 *Phys. Rev. Appl.* **6** 044008
[10] Yariv A, Quantum Electronics, 3rd Edition, ISBN: 978-0-471-60997-1, January 1991
[11] Karpov D V and Horak P (2022) *Phys. Rev. A* **105** 023515
[12] Bäck T., Evolutionary Algorithms in Theory and Practice: Evolution Strategies, Evolutionary Programming, Genetic Algorithms, Oxford Univ. Press 1996
[13] Eiben A E, Smith J E, Introduction to Evolutionary Computing, Springer 2003
[14] Ginzburg P, Berkovitch N, Nevet A, Shor I, and Orenstein M 2011 *Nano Letters* **11** 2329-2333
[15] Liu C, Maier S A, Li G. 2020 *ACS Photonics* **7** 1716-1722
[16] Blechman Y, Almeida E, Sain B, Prior Y 2019 *Nano Letters* **19** 261-268.
[17] Vuckovic J 2017, in Quantum Optics and Nanophotonics, edited by C. Fabre, V. Sandoghdar, N. Treps, and L. F. Cugliandolo, Oxford University Press
[18] Podoliak N, Takahashi H, Keller M, and Horak P 2017 *J. Phys. B.* **50** 085503
[19] Kleckner D, Irvine W T M, Oemrawsingh S S R and Bouwmeester D 2010 *Phys. Rev. A* **81** 043814
[20] Lax M, Louisell W H, and McKnight W B 1975 *Phys. Rev. A* **11** 1365
[21] Chrabaszcz P, Loshchilov I, Hutter F 2018 *Proc. Twenty-Seventh International Joint Conference on Artificial Intelligence (IJCAI-18)* pp 1419–1426 DOI:10.24963/ijcai.2018/197
[22] Zhang X, Clune J, Stanley K O 2017 arXiv:1712.06564
[23] Hunger D, Steinmetz T, Colombe Y, Deutsch C, Hänsch T W and Reichel J 2010 *New J. Phys.* **12** 065038
[24] Gulati G K, Takahashi H, Podoliak N et al. 2017 *Sci Rep* **7** 5556

[25] Benedikter J, Hümmer T, Mader M, Schlederer B, Reichel J, Hänsch T W and Hunger D 2015 *New J. Phys.* **17** 053051
[26] Brandstätter B, McClung A, Schüppert K, et al. 2013 *Rev. Sci. Instr.* **84** 123104
[27] Zoller P et al. 2005 *Eur. Phys. J. D* **36** 203
[28] Häffner H, Roos C, and Blatt R 2008 *Phys. Rep.* **469** 155
[29] Leibfried D et al. 2003 *Nature (London)* **422** 412
[30] Ritter S et al. 2012 *Nature (London)* **484** 195
[31] Kuhn A 2015 "Cavity Induced Interfacing of Atoms and Light", in Engineering the Atom-Photon Interaction: Controlling Fundamental Processes With Photons, Atoms and Solids. Berlin, Germany: Springer; ISBN 978-3-319-19231-4
[32] Hunger D, Deutsch C, Warburton R and Reichel 2012 *AIP Advances* **2**, 012119
[33] Vernooy D W, Furusawa A, Georgiades N P, Ilchenko V S and Kimble H J 1998 *Phys. Rev. A* **57** R2293
[34] Armani D K, Kippenberg T J, Spillane S M and Vahala K J 2003 *Nature* **421** 925
[35] Brinksmeier E and Preuss W 2012 *Phil. Trans. R. Soc. A.* **370** 3973–3992
[36] Gao S, Huang H 2017 *Front. Mech. Eng.* **12** 18–32
[37] Schneider F, Das J, Kirsch B et al. 2019 *Int. J. of Precis. Eng. and Manuf.-Green Tech.* **6** 601–610